



Aalborg Universitet

AALBORG UNIVERSITY  
DENMARK

## **A Direct Maximum Power Point Tracking Method for Single-Phase Grid Connected PV Inverters**

EL Aamri, Faicel; Maker, Hattab; Sera, Dezso; Spataru, Sergiu; Guerrero, Josep M.; Mouhsen, Azeddine

*Published in:*  
IEEE Transactions on Power Electronics

*DOI (link to publication from Publisher):*  
[10.1109/TPEL.2017.2780858](https://doi.org/10.1109/TPEL.2017.2780858)

*Publication date:*  
2018

[Link to publication from Aalborg University](#)

### *Citation for published version (APA):*

EL Aamri, F., Maker, H., Sera, D., Spataru, S., Guerrero, J. M., & Mouhsen, A. (Accepted/In press). A Direct Maximum Power Point Tracking Method for Single-Phase Grid Connected PV Inverters. IEEE Transactions on Power Electronics. DOI: 10.1109/TPEL.2017.2780858

### **General rights**

Copyright and moral rights for the publications made accessible in the public portal are retained by the authors and/or other copyright owners and it is a condition of accessing publications that users recognise and abide by the legal requirements associated with these rights.

- ? Users may download and print one copy of any publication from the public portal for the purpose of private study or research.
- ? You may not further distribute the material or use it for any profit-making activity or commercial gain
- ? You may freely distribute the URL identifying the publication in the public portal ?

### **Take down policy**

If you believe that this document breaches copyright please contact us at [vbn@aub.aau.dk](mailto:vbn@aub.aau.dk) providing details, and we will remove access to the work immediately and investigate your claim.

# A Direct Maximum Power Point Tracking Method for Single-Phase Grid Connected PV Inverters

Faïcel EL Aamri, Hattab Maker, Dezso Sera, *Senior Member, IEEE*, Sergiu Spataru, Josep M. Guerrero, *Fellow, IEEE*, Azeddine Mouhsen

**Abstract**— A direct maximum power point tracking (MPPT) method for PV systems has been proposed in this work. This method solves two of the main drawbacks of the Perturb and Observe (P&O) MPPT, namely: i) the tradeoff between the speed and the oscillations in steady-state, ii) and the poor effectiveness in dynamic conditions, especially in low irradiance when the measurement of signals becomes more sensitive to noise. The proposed MPPT is designed for single-phase single-stage grid-connected PV inverters, and is based on estimating the ripple of the instantaneous PV power and voltage, using a second-order generalized integrator-based quadrature signal generator (SOGI-QSG).

We analyzed the global stability of the closed-loop control system and validated the proposed algorithm through simulation and experiments on an inverter test platform according to the EN 50530 standard. The experimental results confirm the performance of the proposed method in terms of both speed and tracking efficiency.

**Index Terms**—Single stage PV Inverter, Lyapunov Stability, MPPT, P&O, EN 50530 standard.

## I. INTRODUCTION

One crucial component of the control system of any PV inverter is the maximum power point tracking (MPPT) algorithm, which controls the inverter power extraction and operation on the PV array's non-linear current-voltage (I-V) characteristic curve. As an added complexity, the PV array's I-V characteristic is highly dependent on the incident solar irradiance and cell temperature. Therefore, fast changes in irradiance conditions due to moving clouds, cause fast changes in the maximum power point location on the I-V curve, which requires an efficient MPPT algorithm [1-3].

The Perturb and Observe (P&O) is one of the most popular MPPT algorithms, due to its simplicity, ease of implementation, and because it does not require any information about the PV array [4]. The basic algorithm uses a fixed voltage step to increase or decrease the PV array voltage, afterwards, the algorithm compares the current PV array power ( $P_{pv}[k]$ ), with

its previous value, where  $\Delta P = P_{pv}[k] - P_{pv}[k-1]$ . If the power increases  $\Delta P > 0$ , the algorithm continues to perturb the system in the same direction, alternatively if the power decreases  $\Delta P < 0$ , the system will be perturbed in the opposite direction. This process is repeated at each MPP tracking cycle until the MPP is accomplished  $\Delta P \approx 0$ .

However, the P&O algorithm has two main drawbacks: the MPP tracking speed and the efficiency in dynamic irradiance conditions [5]. First, the MPP tracking speed can be increased by using a bigger voltage step to perturb the PV array voltage, however this will increase power loss due to oscillations around the MPP, whereas a smaller step reduces the oscillations, but it will take a longer time to reach the MPP [6-7]. To overcome the tradeoff between the speed and the oscillations, a variable step perturbation for P&O is proposed in [8], but it gives no remarkable improvement. An incremental conductance algorithm (IncCond) has been proposed in [9], however that is essentially the same algorithm as P&O.

The second issue is the poor tracking efficiency in dynamic conditions - rapidly changing solar irradiance. The P&O may track the MPP in the wrong direction, consequently the efficiency deteriorates. A solution for this issue has been presented in [5], where an improved version of the P&O is proposed. In [10] the authors proposed a multisampling P&O as an improvement, but it reaches MPP slowly in the start-up phase, as its principle requires to perform three iterations; increase the voltage with a fixed step, decrease it and increase it again (+++). The work in [11] proposes a model predictive control (MPC) as a solution, however it requires extensive computation and variable inverter switching frequency.

Moreover in paper [12] the authors proposed a ripple correlation control (RCC) method to regulate the maximum power, by means of a 1<sup>st</sup> order high pass filter HPF, used to generate the PV power and the PV voltage ripple. Next, a first order low pass filter is used to determine the sign of the product of power and voltage ripple, necessary as a reference voltage for the conventional DC link voltage controller. The main drawback of this method is a slow response under sudden and large variations of the solar irradiance [13].

However, as described in Fig. 1 the main components of the topology used in this paper are a voltage source inverter, an output filter and a transformer for the isolation function. The output filter is essential, it is needed to filter out the switching frequency harmonics. Regardless the type of the filter (L, LC or LCL), the purpose of the output filter is to ensure the

F. EL Aamri and Az. Mouhsen are with Univ Hassan 1, LRMI, FSTS, 26000 Settati, Morocco (e-mail: f.elaamri@gmail.com; az.mouhsen@gmail.com).

H. Maker is with Univ Hassan 1, LISA, ESTB, 26000 Settati, Morocco (e-mail: hattabmaker@gmail.com).

D. Sera, S. Spataru and J. M. Guerrero are with the Department of Energy Technology, Aalborg University, DK-9220 Aalborg, Denmark (e-mail: des@et.aau.dk; ssp@et.aau.dk; joz@et.aau.dk).

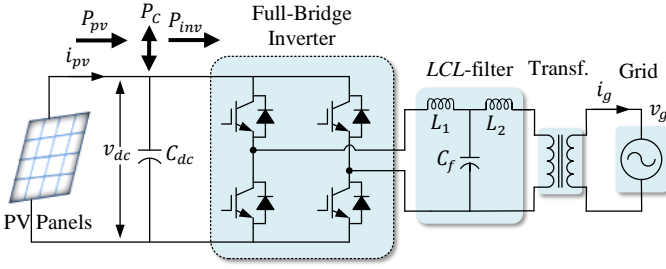


Fig. 1. System configuration of single-stage single-phase grid-connected PV system.

grid injected current has low total harmonic distortion (THD) and will not affect the energy transfer between the DC source and the AC grid. As for the DC link capacitor its main purpose is to store the energy extracted from the PV generator and smooth the DC link voltage ripple.

In the literature the most common control structure for this topology as shown in the Fig. 2 is an MPPT algorithm [14-19], the DC link voltage controller, the current controller and the synchronization algorithm based on Phase Locked Loop - PLL [20]. It should be noted that the DC link capacitor behaves as a temporary energy storage device with the amount of energy stored proportional to the DC voltage. Thus, to consider the stability of the whole controller for single stage grid-connected PV inverter, the quadratic Lyapunov function should be formed based on the energy variation across the DC link capacitor.

In addition, indeed all works that have been done in the literature for single stage grid-connected PV inverter ignore to take into consideration the stability on charging and discharging the DC link capacitor. In the paper [21] the authors use a Lyapunov function in current controller to improve the nonlinear control, rendering the closed-loop globally asymptotically stable. In this case the quadratic Lyapunov function is formed by the balance energy stored in the inductor and the capacitor, but the main disadvantage of this method is that it needs a more oversized system, especially the DC link capacitor.

In this work, we propose a direct MPPT control scheme for single-phase single-stage grid-connected PV inverters that solves both P&O drawbacks: i) ensuring a fast tracking with considerably reduced oscillations in steady-state, ii) and improved efficiency under rapidly changing irradiance.

The proposed method is based on the quadratic Lyapunov function without using a generic MPPT algorithm; it uses the instantaneous PV power ripple  $\tilde{P}_{pv}$  and the instantaneous PV voltage ripple  $\tilde{V}_{pv}$  across the DC link capacitor. The ratio of  $\tilde{P}_{pv}/\tilde{V}_{pv}$  determines the position of the operating point on the P-V curve. Thereafter, the ratio result  $dP/dV$  is multiplied by a gain  $K$  in order to regulate the power fed into the grid.

The remainder of this paper is organized as follows: in section II, the mathematical model of the proposed controller is presented, which is based on the quadratic Lyapunov function that is formed by the variation of the stored energy across the DC link capacitor. In section III the simulation results using both methods are presented, whereas the experimental setup and results are shown in section IV. The conclusions are

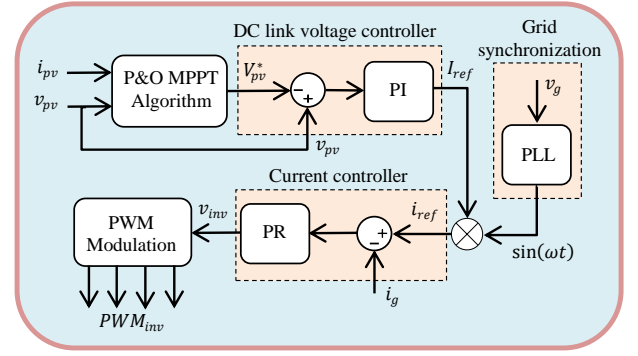


Fig. 2. Control structure for single-stage single-phase grid-connected PV inverter (PI - Proportional Integral, PR - Proportional Resonant, PWM - Pulse Width Modulation).

presented and summarized in section V.

## II. CONTROL STRATEGY

### A. Power Flow Description

Considering the single-stage single-phase grid connected photovoltaic inverter as shown in Fig. 1, and assuming no power losses in the inverter, DC link capacitor and output filter, (so that the other terms accounting for the conduction losses can be neglected to obtain a simple expression), the equation describing the power balance in the DC link can be written as:

$$P_{pv}(t) = P_c(t) + P_{grid}(t) \quad (1)$$

The power fed into the grid  $P_{grid}$  is equal to:

$$P_{grid}(t) = v_g i_g = V_g I_g (1 - \cos 2\omega t) \quad (2)$$

Where  $v_g$  and  $i_g$  are the instantaneous grid voltage and grid current respectively.  $I_g$  is the root mean square (RMS) of the injected current,  $V_g$  is the RMS of the grid voltage, and  $\omega$  is the grid pulsation. The power injected into single phase grid  $P_{grid}$ , calculated as in (2), follows a sinusoidal waveform with twice the grid frequency. The PV generator could not be operated at the MPP if this pulsating power is not decoupled by means of an energy buffer. Therefore, a capacitor bank is typically used for buffering this energy.

The  $P_c(t)$  is the instantaneous power flow in the DC link capacitor and is equal to:

$$P_c(t) = C_{dc} V_{dc} \frac{dV_{dc}}{dt} \quad (3)$$

The average power  $P_{av}$  fed into the grid can be written as:

$$P_{av} = \frac{1}{T_{grid}} \int_0^{T_{grid}} V_g I_g (1 - \cos 2\omega t) dt = V_g I_g \quad (4)$$

Where  $T_{grid}$  is the grid voltage period.

### B. Proposed Controller

The control system of the PV inverter can be divided into three parts: i) DC link voltage controller, ii) current controller, iii) and grid synchronization controller. The DC link voltage controller is used to regulate the DC voltage at a desirable level for extracting the maximum power from the PV array.

Considering that the PV characteristic is nonlinear, while the irradiance changes, the DC power will change accordingly, consequently, the MPP will also shift. In this case, since the grid voltage is fixed (this can be assumed in most cases), the power transferred to the grid is controlled only by the inverter output current.

The mathematical model describing the dynamics of the power flow is given by (5), where  $I_g^*$  represents the reference grid current of the inverter:

$$V_g I_g^* = I_{pv} V_{pv} - C_{dc} V_{dc} \frac{dV_{dc}}{dt} \quad (5)$$

Where  $V_{pv}$  and  $I_{pv}$  are periodic signals having the average components  $\bar{V}_{pv}$ ,  $\bar{I}_{pv}$  and the AC components  $\tilde{v}_{pv}$ ,  $\tilde{i}_{pv}$  with oscillation period  $T = 1/(2f_{grid})$ , and defined respectively as:

$$\begin{cases} V_{pv} = \bar{V}_{pv} + \tilde{v}_{pv} \\ I_{pv} = \bar{I}_{pv} + \tilde{i}_{pv} \end{cases} \quad (6)$$

The power injected into the grid  $P_{av}$  is controlled according to (7), using a feed-forward power  $P_{pv}$  term, and a second term  $K dP/dV$  accounting for the dynamics of the PV inverter system:

$$P^* = P_{pv} + K \frac{dP}{dV} \quad (7)$$

Where  $P^*$  represents the reference power and  $K$  is a constant parameter which allows adjusting the amount of power in the controller to follow the maximum power point, and it will be discussed in detail later on. Hence, substituting (7) into (5) yields:

$$V_g I_g^* = P_{pv} + K \frac{dP}{dV} \quad (8)$$

And by substituting (8) into (5) we get:

$$C_{dc} V_{dc} \frac{dV_{dc}}{dt} = -K \frac{dP}{dV} \quad (9)$$

Based on equation (9), we can deduce that the  $dP/dV$  is related to the DC link capacitor dynamics.

The estimation method of the AC components (ripples) of the PV power  $\tilde{p}_{pv}$  and the DC link voltage  $\tilde{v}_{dc}$ , is based on a second-order generalized integrator-based quadrature signal generator (SOGI-QSG) [22], as presented in Fig. 3, and defined by the closed-loop transfer function in (10):

$$F(s) = \frac{\omega_n s}{s^2 + \omega_n s + \omega_n^2} \quad (10)$$

Where  $\omega_n$  represents the resonance frequency, equal to double the grid frequency.

Fig. 4 shows the proposed control strategy. The computed value of the reference current is determined using the PV Power reference generated by the proposed controller as shown in Fig. 3 and the RMS value of the grid voltage. The PLL extracts the phase angle of the grid voltage and is multiplied by the magnitude of the reference grid current. Then, the current controller is proceeding to regulate the grid current  $i_g$ .

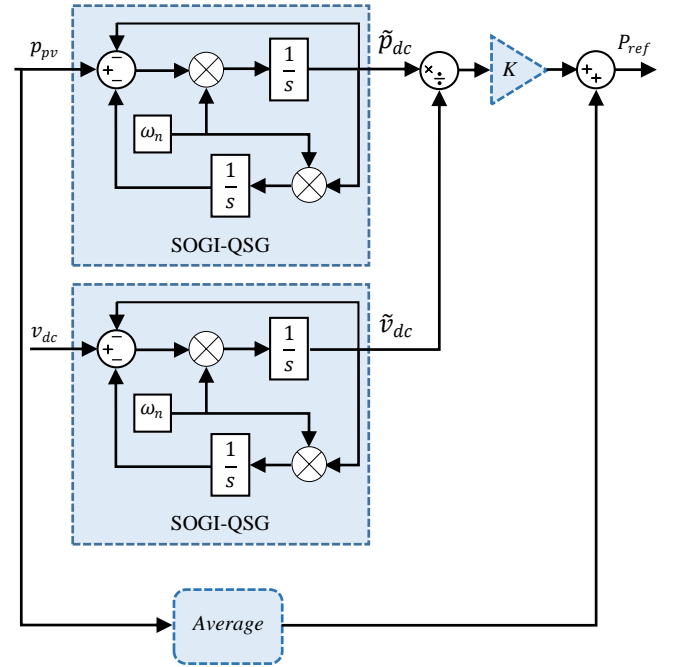


Fig. 3. Generation of reference power using SOGI-QSG.

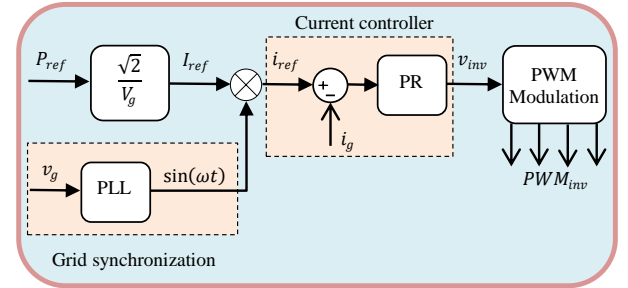


Fig. 4. Overall controller configuration using the proposed reference power as input and using unipolar PWM.

### C. Stability analysis

The stability of the closed loop system will be determined primarily by the sign and magnitude of the controller parameter  $K$ . To determine the sign of the parameter  $K$ , we use Lyapunov's stability theorem to study the overall system's stability. According to [23] the Lyapunov function  $V(x)$  is a scalar energy function, the system is globally asymptotically stable if  $V(x)$  satisfies that  $V(0) = 0$ , and  $V(0) > 0$  for all  $x \neq 0$  and  $\frac{dV(x)}{dt} < 0$  for all  $x \neq 0$ .

To achieve this, we derive the quadratic Lyapunov function  $V(E_n)$  as in (11), based on the energy variation across the DC link capacitor, and assuming that the energy stored in the grid filter can be neglected:

$$V(E_n) = \frac{C^2}{4} (V_{dc}^{*2} - V_{dc}^2)^2 \quad (11)$$

Where  $E_n$  refers the energy stored in DC link capacitor and  $V_{dc}^*$  is the reference DC link voltage.

To ensure global stability of the dynamic system, the condition  $V(E_n)\dot{V}(E_n) < 0$  must hold for all  $E_n \neq 0$ . Consequently,  $V(E_n) > 0$  and  $\dot{V}(E_n) < 0$ , where:

$$\frac{dV(E_n)}{dt} = \frac{C^2}{2} (V_{dc}^{*2} - V_{dc}^2) \left( 0 - 2V_{dc} \frac{dV_{dc}}{dt} \right) \quad (12)$$

Finally, by arranging the terms it can be obtained as:

$$\frac{dV(E_n)}{dt} = -C^2 V_{dc} \frac{dV_{dc}}{dt} (V_{dc}^{*2} - V_{dc}^2) \quad (13)$$

Therefore, to check the previous condition  $V(E_n)\dot{V}(E_n) < 0$  for the controller stability, and according to (13), if  $V_{dc} > V_{dc}^*$ , and  $\dot{V}(E_n) < 0$ , this implies that  $dV_{dc}/dt < 0$ .

According to (9),  $C_{dc}V_{dc}\frac{dV_{dc}}{dt} < 0$ , which implies that  $-K dP/dV < 0$ .

Therefore, since the operating point is located in the right side because it was assumed that  $V_{dc} > V_{dc}^*$  as shown in Fig. 5, it gives  $dP/dV < 0$ , which means that  $K < 0$ .

The following equation summarizes the proof.

$$\text{if } V_{dc} > V_{dc}^*, \frac{dV(E_n)}{dt} < 0 \Rightarrow \frac{dV_{dc}}{dt} < 0 \Rightarrow K < 0 \quad (14)$$

As for the other case, if  $V_{dc} < V_{dc}^*$ , and since  $\dot{V}(E_n)$  is also negative, this implies that  $dV_{dc}/dt > 0$ .

According to equation (9),  $C_{dc}V_{dc}\frac{dV_{dc}}{dt} > 0$ , resulting that  $-K \frac{dP}{dV} > 0$ .

Therefore, since the operating point is located in the left side because it was assumed that  $V_{dc} < V_{dc}^*$  as shown in Fig. 5, it gives that  $dP/dV > 0$ , which means that  $K < 0$ .

The following equation summarizes the proof.

$$\text{if } V_{dc} < V_{dc}^*, \frac{dV(E_n)}{dt} < 0 \Rightarrow \frac{dV_{dc}}{dt} > 0 \Rightarrow K < 0 \quad (15)$$

However, it should be mentioned that during normal operation, the system will be subject to disturbances. The DC link capacitor is used as a damping element to maintain the stability for the MPPT and the grid-connected inverter during these transitory states.

The DC link capacitor is sized based on the allowable magnitude of the PV voltage ripple, therefore the PV power can be written as the equation below:

$$P_{pv} = 2\pi f_{grid} \cdot C_{dc} \cdot V_{dc} \cdot \Delta V_{dc} \quad (16)$$

As shown in (16), the DC link voltage ripple depends on the parameters;  $P_{pv}$  and  $V_{dc}$ , which are related to the PV characteristic, to designate the capacitor value, it should be taken into consideration the low irradiation, in this case the PV power decreases considerably than the PV voltage, which impose to size the capacitor based on low irradiation in order to keep  $\Delta V_{dc}$  distinctive on the noise measurement.

As a consequence, the minimum capacitance required for this amount of the power and the DC link voltage ripple is determined as follows:

$$C_{dc} = \frac{P_{pv}}{2\pi f_{grid} \cdot V_{dc} \cdot \Delta V_{dc}} \quad (17)$$

In this paper,  $\Delta V_{dc}$  is set to 6V at standard test conditions (STC). In addition, the parameter  $K$  should be calculated

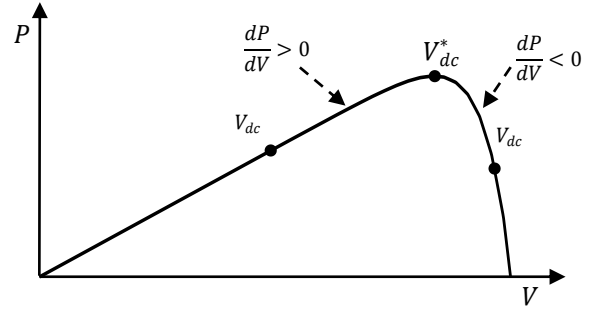


Fig. 5. Movement of the operating point on P-V characteristic.

carefully for a given system to avoid the risk of operating the system in an unstable state.

Next, we can reformulate equation (7) as:

$$P^* = P_{pv} + \Delta P^* \quad (18)$$

Where  $\Delta P^*$  is the power adjustment, that controls the speed to reach the maximum power point. As long as  $\Delta P^*$  increases, the MPPT speed becomes faster, while the stability margin of the whole system decreases. Its expression contains two parameters, the first one is a constant  $K$  and the second one is a variable ratio  $dP/dV$  that depends on the operating point on the P-V curve.

To ensure the stability PV inverter system in the entire solar irradiation range (0 to 1000 W/m<sup>2</sup>), as a  $K$  is just a constant, we will focus on the variable ratio  $dP/dV$ .

In the vicinity of the MPP, the variation of  $P$ , can be expressed as:

$$\dot{P} \approx \Delta (I_{MPP} \cdot V_{MPP}) = V_{MPP} \cdot \dot{I}_{pv} + I_{MPP} \cdot \dot{V}_{pv} + \dot{V}_{pv} \cdot \dot{I}_{pv} \quad (19)$$

By arranging the terms, we can get:

$$\frac{\dot{P}}{\dot{V}_{pv}} = V_{MPP} \frac{\dot{I}_{pv}}{\dot{V}_{pv}} + I_{MPP} + \dot{I}_{pv} \quad (20)$$

Based on [24], it can be assumed that:

$$\left. \frac{\dot{I}_{pv}}{\dot{V}_{pv}} \right|_{MPP} = - \frac{I_{MPP}}{V_{MPP}} \quad (21)$$

Substituting (21) into (20) we get:

$$\frac{\dot{P}}{\dot{V}_{pv}} = \dot{I}_{pv} \quad (22)$$

And by substituting (22) into (21) we get:

$$\frac{\dot{P}}{\dot{V}_{pv}} = - \frac{\dot{V}_{pv} \cdot I_{MPP}}{V_{MPP}} \quad (23)$$

In the equation above we substitute the value of  $\Delta V$  in (16), as a result we get:

$$\frac{dP}{dV} = - \frac{1}{2\pi \cdot f_{grid} \cdot C_{dc}} \frac{P_{MPP}^2}{V_{MPP}^3} \quad (24)$$

According to the equation (24), the Fig. 6 shows the

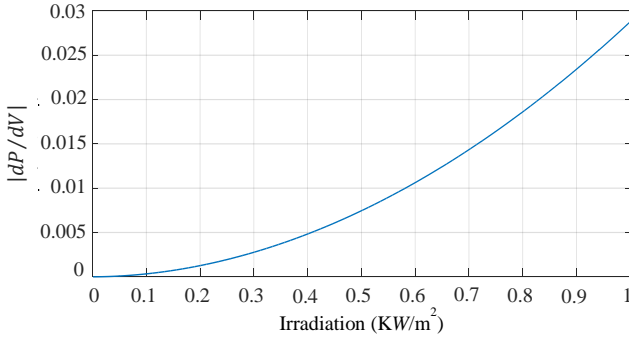


Fig. 6. Absolute value of  $dP/dV$  near MPP versus irradiance.

absolute value of  $dP/dV$  at the maximum power point for nominal power of 1 kW in each irradiance level; it can be seen that as the irradiance decreases, the ratio decreases accordingly, owing to the more considerable drop of the PV power than the PV voltage. Which means that if the parameter  $K$  is designed for standard test conditions at  $1 \text{ kW}/\text{m}^2$  irradiance such that the stability criterion is fulfilled in those conditions, the system will remain stable in all lower irradiance levels, without adjusting the parameter.

On the other hand, based on the equations (18) and (24), in the steady-state at the vicinity of the MPP, the oscillation of the PV power can be written as:

$$\Delta P|_{MPP} = -\frac{K}{2\pi \cdot f_{grid} \cdot C_{dc}} \frac{P_{MPP}^2}{V_{MPP}^3} \quad (25)$$

Which means that increasing the parameter  $K$  in the proposed controller, the MPP will be reached faster, obviously at a certain limit, increasing  $K$  does not yield significant improvements in speed, however if  $K$  is oversized, it will cause more power oscillations, as shown in Fig. 7.

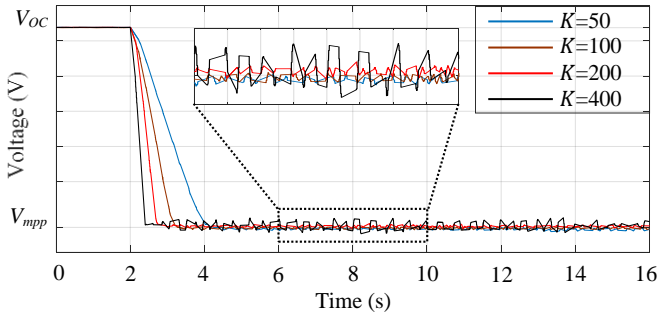


Fig. 7. Experimental PV voltage waveforms after startup showing the convergence to MPP with different  $K$  values.

With regard to partially shaded condition (PSC), the proposed method will behave similarly to P&O, i.e. will track the nearest MPP. The advantage of this method is the fast tracking. PS detection and tracking features (such as I-V scan) can be added in a similar manner as for the P&O. However, we consider PS detection and tracking as outside the scope of this paper, since they are not specific to the proposed method.

### III. SIMULATION STUDY

TABLE 1. Parameters for simulation and experiment.

PV power	1 kW
$V_{mpp}$	455 V
$I_{sc}$	2.42 A
$V_{oc}$	568 V
DC link Capacitor	1200 $\mu\text{F}$
Switching frequency	8000 Hz
LCL-filter	$L_1 = 2.6 \text{ mH}$ ; $C_f = 2.2 \mu\text{F}$ ; $L_2 = 0.41 \text{ mH}$ ;
Grid nominal voltage (RMS)	230 V
Grid nominal frequency	50 Hz

The proposed control strategy has been evaluated and compared to the conventional P&O, through simulation in Matlab/Simulink, for a single-stage single-phase grid connected PV inverter. The parameters of PV system used in the simulation and experimental tests are summarized in the Table 1.

#### A. Test case 1 – Steady-state conditions

The first test case aims to evaluate the tracking efficiency of the proposed MPPT, under standard atmospheric test constant at  $1000 \text{ W}/\text{m}^2$  and  $25^\circ\text{C}$  respectively, at this level of the irradiance, the simulated PV array has a MPP of  $\sim 1 \text{ kW}$ . The parameters P&O MPPT are:  $f_{MPPT} = 10 \text{ Hz}$  – tracking frequency, and  $\Delta V = 1 \text{ V}$  - increment step voltage, which were chosen to reduce the losses caused by permanent oscillations around the correct value of the MPP [25].

Fig. 8 shows the operation of the two MPPT control algorithms side by side. Both the proposed MPPT method (shown in red) and P&O (blue) start at time 0.4 s, which is the time when the DC link capacitor has been completely charged, and its voltage is equal to open circuit voltage of the PV generator.

As can be observed, the proposed method reaches the MPP first and very fast, with a response time of only  $t_r = 0.025 \text{ s}$ , compared to P&O that converges with a fixed step and a response time equal to  $t_r = 11.3 \text{ s}$ . Moreover, we can observe that the P&O has slightly larger oscillations near the MPP voltage  $V_{mpp} = 455$  - oscillating in the interval [451.5V 459.5V], compared to the proposed method, which oscillates in the interval [452V 457.8V]. From here we can conclude that the proposed MPPT method has better instantaneous efficiency in steady state than P&O. Regarding the efficiency, the P&O can also have high efficiency in steady state, however, the speed to reach the MPP will slow down.

#### B. Test case 2 – Dynamic conditions

In the second test case, we analyze the dynamic efficiency of the proposed MPPT compared to P&O. This test considers a variable/trapezoidal solar irradiance profile, with a rate of change of  $100 \text{ W}/\text{m}^2/\text{s}$ , from 30% to 100% of STC irradiance as shown in Fig. 9. Here, the black line represents the maximum power MPP that can be generated by the PV generator. From Fig.9, we see clearly that the change of the solar irradiance has no influence at all on the tracking efficiency for the proposed method, the black line and the red line are overlapped.

As for the P&O method, we can observe in Fig. 10 that when



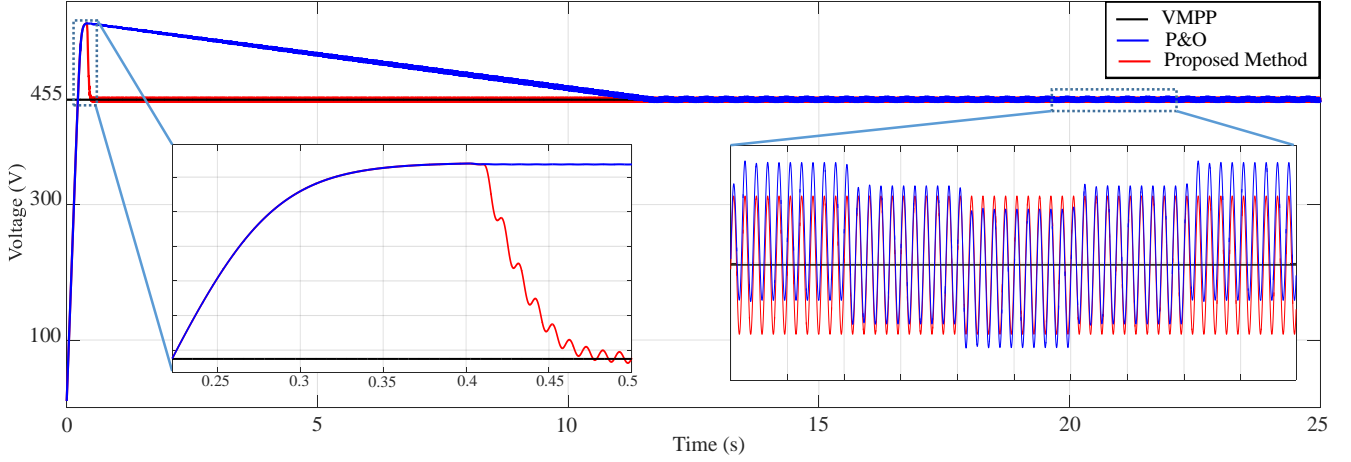


Fig. 8. Start waveforms comparison for DC link voltage.

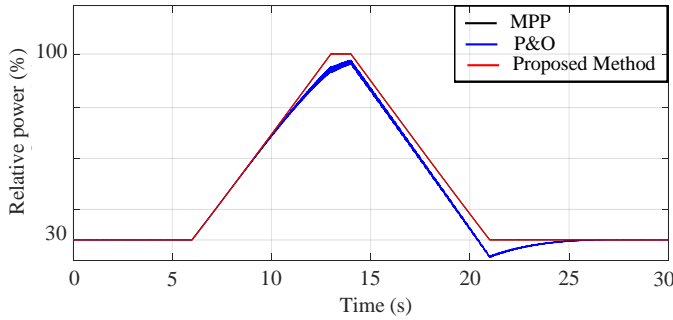


Fig. 9. The output PV power under trapezoidal irradiance profile.

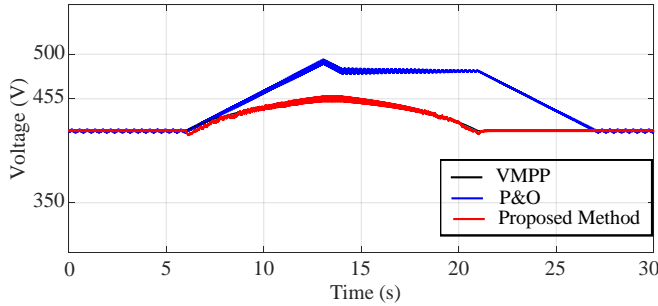


Fig. 10. DC link voltage under trapezoidal irradiance profile.

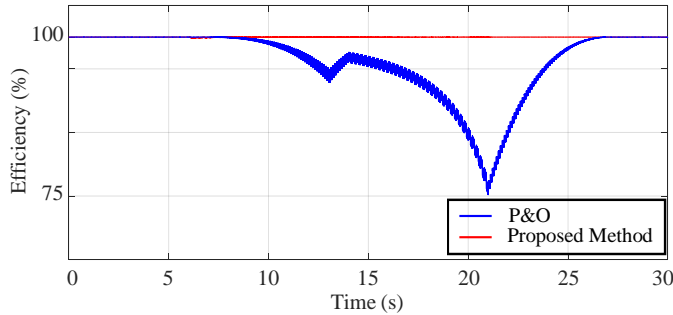


Fig. 11. Instantaneous efficiency under trapezoidal irradiance profile.

the solar irradiance increases, the P&O cannot track the MPP accurately.

Moreover, fig. 11 shows how the instantaneous efficiency of P&O drops about 25%. While the proposed method tracks the MPP with the same efficiency as in the steady-state operation.

#### IV. EXPERIMENTAL VALIDATION

##### A. Experimental setup description

In the experiment study, the test setup (shown in Fig. 12 and Fig. 13) consists of the following components: 1000V/40A high bandwidth PV simulator (Regatron TopCon Quadro with a linear post-processing unit TC.LIN), a 2.2kW Danfoss VLT-FC302 inverter, grid connected through an LCL filter and a 1:1 single phase transformer. The PV simulator emulates a preloaded I-V curve of the PV array. The control structure has been implemented in Simulink, and the dSPACE 1103 Real-Time Control Platform.

As shown in the Fig. 13 the dSPACE controller receives the signal values measured through LEM sensors from the grid voltage, grid current, DC link capacitor voltage and the PV output current.

The parameters used for the PI voltage controller in the conventional method P&O are:

$$\begin{cases} K_{p_{u-dc}} = 8e^{-5} \\ K_{i_{u-dc}} = 8.5e^{-4} \end{cases} \quad (26)$$

As for the proposed method, based on (25), the parameter  $K$  is chosen equal to 200 at standard conditions.

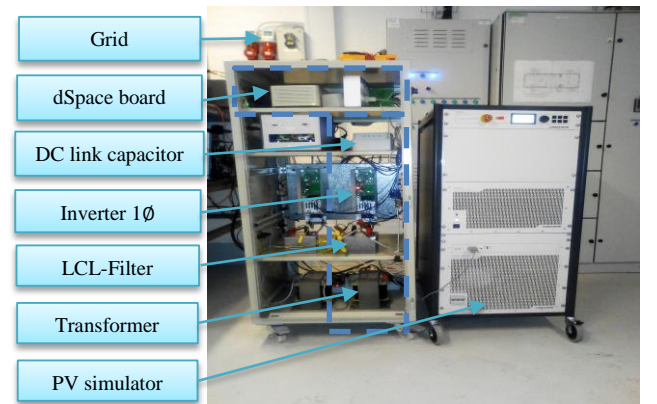


Fig. 12. Photo of the experimental setup.

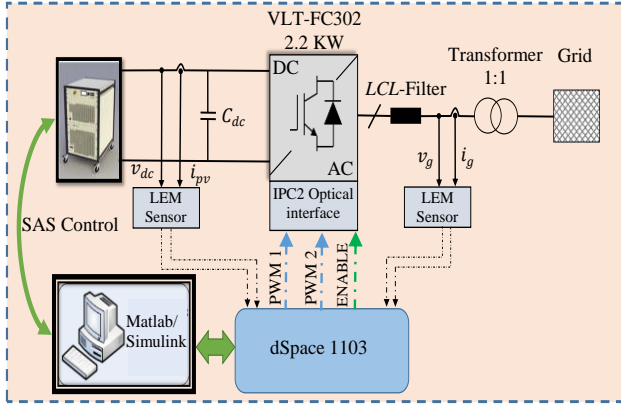


Fig. 13. Layout of the experimental setup.

### B. Experiment results

To verify the simulation results, different laboratory tests were carried out in the same conditions as used in simulation. Fig. 14 shows the first experiment results that demonstrates the ability of the MPPT to reach and keep the MPP under steady-state conditions. The MPPT in both the direct reaching and P&O test case, is enabled at  $t_0 = 5.6$  s. From Fig.14 we observe that the proposed method takes  $\sim 0.6$  s to reach the MPP, while P&O takes  $\sim 11.3$  s.

Fig. 15 shows the voltage response starting at time  $t_0 = 5.6$  s and  $V_{oc} = 568$  V.

In both cases the MPPT reaches  $V_{mpp} = 455$  V but at different times. Moreover, we remark the larger oscillations around the  $V_{mpp}$  in the case of the P&O, compared to the

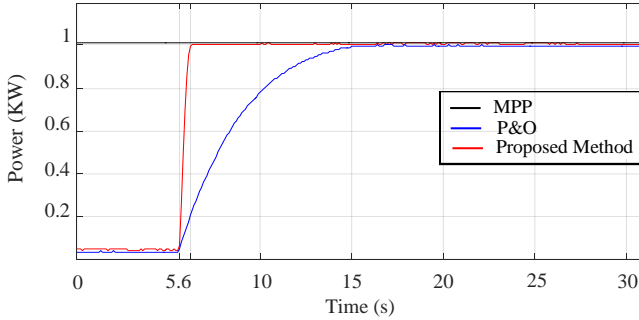


Fig. 14. Experimental start waveforms of PV power for both methods.

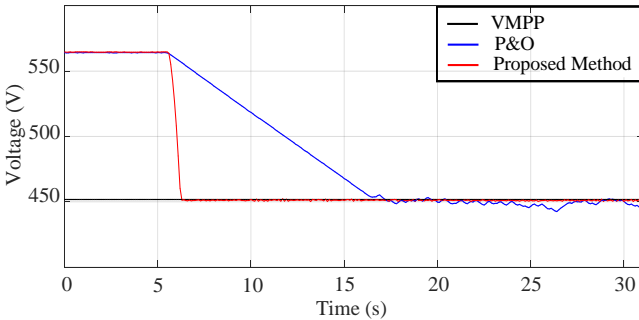


Fig. 15. Experimental start waveforms comparison of DC link voltage.

direct MPP reaching method. These findings match the simulation results, indicating that the P&O has less instantaneous efficiency compared to the proposed method.

The second experimental test case, evaluates the dynamic efficiency of two MPPs for a trapezoidal solar irradiance profile with  $100 \text{ W/m}^2/\text{s}$  slope. Fig. 16 and Fig 17 show that the proposed MPPT tracks the maximum power very well, even in dynamic conditions. By comparison, the P&O fails to track the MPP accurately, having a dynamic efficiency of  $\eta=92.97\%$ , compared to the proposed MPPT of  $\eta=99.8\%$ .

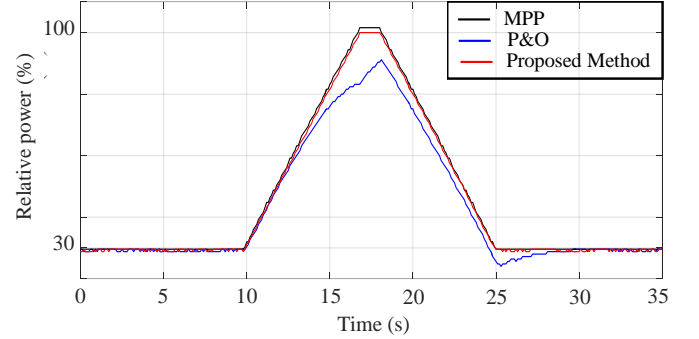


Fig. 16. Experimental results of PV power under trapezoidal irradiance profile.

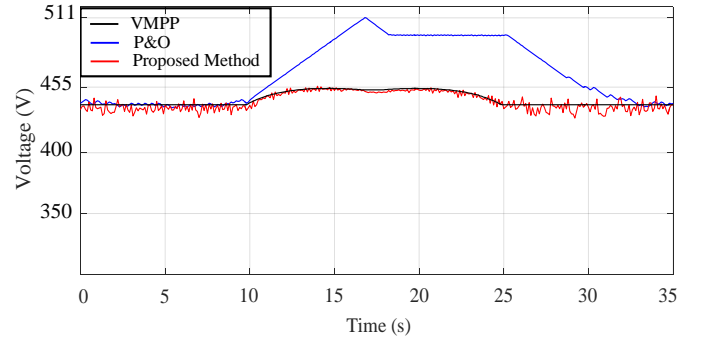


Fig. 17. Experimental results for DC link voltage under trapezoidal irradiance profile.

### C. EN 50530 test

The final experiment test aims to evaluate the MPPT efficiency according to the EN 50530 inverter test standard for static and dynamic conditions [26]. In static conditions, the EN 50530 standard evaluates the MPPT efficiency at different power levels, according to European efficiency  $\eta_{EUR}$  and Californian efficiency  $\eta_{CEC}$ :

$$\eta_{EUR} = 0.03.\eta_{5\%} + 0.06.\eta_{10\%} + 0.13.\eta_{20\%} + 0.1.\eta_{30\%} + 0.48.\eta_{50\%} + 0.2.\eta_{100\%} \quad (27)$$

$$\eta_{CEC} = 0.04.\eta_{10\%} + 0.05.\eta_{20\%} + 0.12.\eta_{30\%} + 0.21.\eta_{50\%} + 0.53.\eta_{75\%} + 0.05.\eta_{100\%} \quad (28)$$

Where the  $\eta_{5\%}$ ,  $\eta_{10\%}$  and so on in the equations refer to MPPT efficiency at  $i\%$  of standard test conditions (STC). The equivalent static efficiencies can be calculated as bellow:

$$\eta_{stat,i} = \frac{\sum_i P_{PV,meas} \cdot \Delta T}{P_{mp} \cdot T_M} \quad (29)$$

Where  $P_{PV,meas}$  is the measured DC inverter power in each sampling time  $\Delta T$ ,  $P_{mp}$  is the maximum power of the PV array,



$T_M$  represents the whole sampling time of the measurement, and  $i$  is the power level for 5%, 10% and so on.

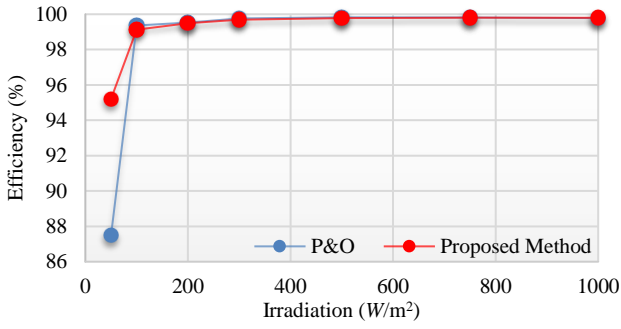


Fig. 18. Efficiency under static irradiance for both methods.

Fig. 18 shows the efficiency for both MPPT methods under a wide range of irradiance conditions from 50 to 1000 W/m². It shows that they exhibit a similar performance during high irradiance conditions, while the proposed method performance exceeds that of P&O at low irradiance levels. In this case, the PV array's power-voltage characteristic is flatter, and the P&O method becomes more sensitive to measurement noise, as a consequence, the P&O's efficiency decreases down to 87.48% for 50 W/m². The following Table 2 summarizes the experiment results for the proposed method and P&O. It can be seen from the comparison that the efficiencies of both methods are extremely close according to Californian efficiency  $\eta_{CEC}$ , while according to European efficiency  $\eta_{EUR}$  the proposed method is slightly better than P&O.

TABLE 2. Experimental results under static irradiance according to EN 50530.

	$\eta_{EUR}$	$\eta_{CEC}$
Direct MPPT	99.56	99.75
P&O	99.38	99.78

In the dynamic test, the MPP changes due to trapezoidal irradiance profile variation, in two sequences: i) the first one from 10% to 50% of STC irradiance; ii) and the second from the 30% to 100% of STC irradiance, as described in Table 3 and Table 4, and as shown in Fig. 19 and Fig. 20.

TABLE 3. Description of the trapezoidal irradiance profile from 10% to 50% of STC irradiance according to EN 50530.

Sequence number	Repetition	Rise time [s]	Wait [s]	Fall time [s]	Wait [s]
1	2	80	10	80	10
2	2	40	10	40	10
3	3	20	10	20	10
4	4	13.3	10	13.3	10
5	6	8	10	8	10

TABLE 4. Description of the trapezoidal irradiance profile from 30% to 100% of STC irradiance according to EN 50530.

Sequence number	Repetition	Rise time [s]	Wait [s]	Fall time [s]	Wait [s]
1	5	70	10	70	10
2	5	50	10	50	10
3	5	35	10	35	10
4	5	23	10	23	10
5	5	14	10	14	10
6	5	7	10	7	10

Each sequence has  $N$  repetitions of the same trapezoidal characteristic. In this case, the equivalent dynamic efficiency can be calculated as below:

$$\eta_{dyn} = \frac{1}{N} \sum_{j=1}^N \eta_{dyn,j} \quad \text{where} \quad \eta_{dyn,j} = \frac{\sum_j P_{PV,meas} \cdot \Delta T}{\sum_j P_{mp} \cdot \Delta T} \quad (30)$$

In this paper, a shortened version of the EN 50530 dynamic test is considered, which takes around one hour and fifteen minutes for checking completely both methods. Fig. 19 shows measured P&O tracked array power (blue) versus the real MPP of the PV array (black).

Similarly, Fig. 20 shows the tracking performance of the proposed MPPT, from where we can observe a higher dynamic efficiency ( $\eta_{dyn} = 99.74\%$ ), compared to P&O ( $\eta_{dyn} = 98.16\%$ ).

Fig. 21 summarizes the efficiency of the two MPPTs during the 5-trapezoidal from low-to-medium irradiance sequences, shown in Fig. 19 and 20. The first two sequences show similar efficiency results, with a difference between them of 0.04%

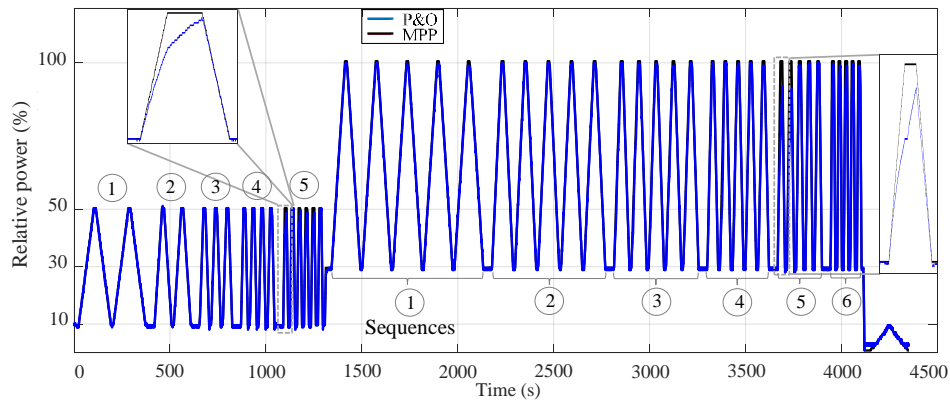


Fig. 19. PV power for P&O under dynamic irradiance profile according to EN 50530.

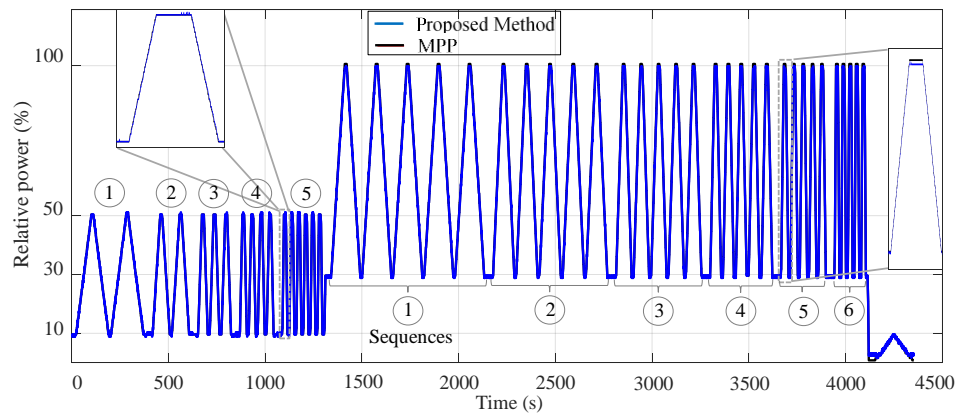


Fig. 20. PV power for the proposed method under dynamic irradiance profile according to EN 50503.

approximately due to very slow ramp speed of 80 s and 40s respectively. Between sequence three and fifth, the efficiency of the P&O drops because of the high speed of the ramp, with 20s, 13.3s, and 8s of each of them respectively.

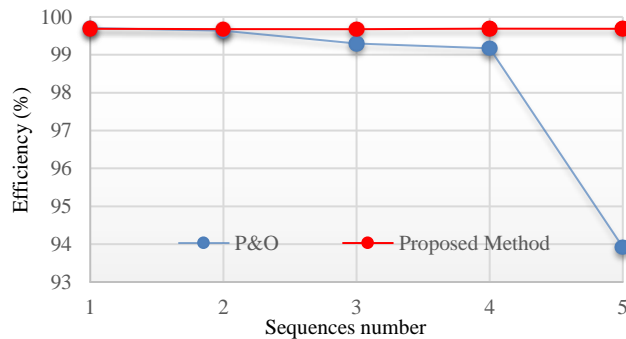


Fig. 21. Efficiency comparison for the both methods from low-to-medium irradiance.

Fig. 22 compares the efficiency of the two MPPTs according to the second part of the EN 50530 test, from medium-to-high irradiance. In each sequence, the proposed method exhibits an efficiency between 99.77% and 99.79%, compared to P&O which shows much lower tracking efficiency in dynamic conditions.

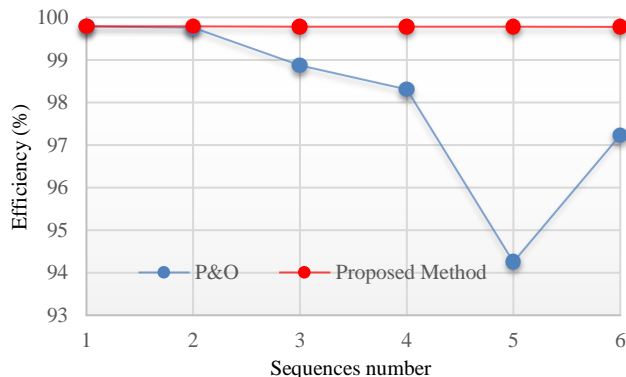


Fig. 22. Efficiency comparison for the both methods from medium-to-high irradiance.

## V. CONCLUSION

This paper has described the design of an effective controller for direct reaching the maximum power point for a single-stage single-phase grid-connected PV inverter. The proposed method has been designed based on the stability analysis using the Lyapunov quadratic function that is formed from the variation of energy stored in the DC link capacitor. From the simulations and experimental results on an advanced test platform and according to the EN 50530 standard, it was confirmed that the proposed method achieves high efficiency in both static and dynamic conditions. Furthermore, the proposed method is very fast to reach the MPP.

## REFERENCES

- [1] T. Kerekes, R. Teodorescu, and U. Borup, "Transformerless Photovoltaic Inverters Connected to the Grid," APEC 07 - Twenty-Second Annual IEEE Applied Power Electronics Conference and Exposition, pp. 1733–1737, 2007.
- [2] I. S. Kim, M. B. Kim, and M. J. Youn, "New Maximum Power Point Tracker Using Sliding-Mode Observer for Estimation of Solar Array Current in the Grid-Connected Photovoltaic System," IEEE Transactions on Industrial Electronics, vol. 53, no. 4, pp. 1027–1035, 2006.
- [3] J. Selvaraj and N. A. Rahim, "Multilevel Inverter For Grid-Connected PV System Employing Digital PI Controller," IEEE Transactions on Industrial Electronics, vol. 56, no. 1, pp. 149–158, 2009.
- [4] M. Rosu-Hamzescu and S. Oprea, "Practical guide to implementing solar panel MPPT algorithms," Microchip Technol. Inc, 2013.
- [5] D. Sera, R. Teodorescu, J. Hantschel, and M. Knoll, "Optimized Maximum Power Point Tracker for Fast-Changing Environmental Conditions," IEEE Transactions on Industrial Electronics, vol. 55, no. 7, pp. 2629–2637, 2008.
- [6] X. Liu and L. A. C. Lopes, "An improved perturbation and observation maximum power point tracking algorithm for PV arrays," 2004 IEEE 35th Annual Power Electronics Specialists Conference (IEEE Cat. No.04CH37551), vol. 3, p. 2005–2010 Vol.3, 2004.
- [7] X. Li, H. Wen, L. Jiang, W. Xiao, Y. Du, and C. Zhao, "An Improved MPPT Method for PV System With Fast-Converging Speed and Zero Oscillation," IEEE Transactions on Industry Applications, vol. 52, no. 6, pp. 5051–5064, 2016.
- [8] S. K. Kollimalla and M. K. Mishra, "Variable Perturbation Size Adaptive P&O MPPT Algorithm for Sudden Changes in Irradiance," IEEE Transactions on Sustainable Energy, vol. 5, no. 3, pp. 718–728, 2014.
- [9] D. Sera, L. Mathe, T. Kerekes, S. V Spataru, and R. Teodorescu, "On the Perturb-and-Observe and Incremental Conductance MPPT Methods for PV Systems," IEEE Journal of Photovoltaics, vol. 3, no. 3, pp. 1070–1078, 2013.
- [10] G. Escobar, S. Pettersson, C. N. M. Ho, and R. Rico, "Multi-sampling maximum power point tracker (MS-MPPT) to compensate irradiance and temperature changes," IEEE Transactions on Sustainable Energy, vol. PP, no. 99, p. 1, 2017.

- [11] M. Metry, M. B. Shadmand, R. S. Balog, and H. Abu-Rub, "MPPT of Photovoltaic Systems Using Sensorless Current-Based Model Predictive Control," *IEEE Transactions on Industry Applications*, vol. 53, no. 2, pp. 1157–1167, 2017.
- [12] D. Casadei, G. Grandi, and C. Rossi, "Single-phase single-stage photovoltaic generation system based on a ripple correlation control maximum power point tracking," *IEEE Transactions on Energy Conversion*, vol. 21, no. 2, pp. 562–568, 2006.
- [13] M. Hammami, G. Grandi, and M. Rudan, "An improved MPPT algorithm based on hybrid RCC scheme for single-phase PV systems," *IECON 2016 - 42nd Annual Conference of the IEEE Industrial Electronics Society*, pp. 3024–3029, 2016.
- [14] M. Ciobotaru, R. Teodorescu, and F. Blaabjerg, "Control of Single-Stage Single-Phase PV Inverter," *EPE J.*, vol. 16, no. 3, pp. 20–26, Sep. 2006.
- [15] F. Paz and M. Ordonez, "Zero Oscillation and Irradiance Slope Tracking for Photovoltaic MPPT," *IEEE Transactions on Industrial Electronics*, vol. 61, no. 11, pp. 6138–6147, 2014.
- [16] J. Ahmed and Z. Salam, "A Modified P&O Maximum Power Point Tracking Method With Reduced Steady-State Oscillation and Improved Tracking Efficiency," *IEEE Transactions on Sustainable Energy*, vol. 7, no. 4, pp. 1506–1515, 2016.
- [17] J. H. Teng, W. H. Huang, T. A. Hsu, and C. Y. Wang, "Novel and Fast Maximum Power Point Tracking for Photovoltaic Generation," *IEEE Transactions on Industrial Electronics*, vol. 63, no. 8, pp. 4955–4966, 2016.
- [18] M. Killi and S. Samanta, "An Adaptive Voltage-Sensor-Based MPPT for Photovoltaic Systems With SEPIC Converter Including Steady-State and Drift Analysis," *IEEE Transactions on Industrial Electronics*, vol. 62, no. 12, pp. 7609–7619, 2015.
- [19] V. Kokaew, S. M. Sharkh, and M. Moshrefi-Torbati, "Maximum Power Point Tracking of a Small-Scale Compressed Air Energy Storage System," *IEEE Transactions on Industrial Electronics*, vol. 63, no. 2, pp. 985–994, 2016.
- [20] M. Ciobotaru, R. Teodorescu, and F. Blaabjerg, "A new single phase PLL structure based on second order generalized integrator," in *Power Electronics Specialists Conference*, 2006, pp. 1–6.
- [21] C. Meza, D. Biel, D. Jeltsema, and J. M. A. Scherpen, "Lyapunov-Based Control Scheme for Single-Phase Grid-Connected PV Central Inverters," *IEEE Transactions on Control Systems Technology*, vol. 20, no. 2, pp. 520–529, 2012.
- [22] S. Golestan, S. Y. Mousazadeh, J. M. Guerrero, and J. C. Vasquez, "A Critical Examination of Frequency-Fixed Second-Order Generalized Integrator-Based Phase-Locked Loops," *IEEE Transactions on Power Electronics*, vol. 32, no. 9, pp. 6666–6672, 2017.
- [23] H. Komurcugil, N. Altin, S. Ozdemir, and I. Sefa, "An Extended Lyapunov-Function-Based Control Strategy for Single-Phase UPS Inverters," *IEEE Transactions on Power Electronics*, vol. 30, no. 7, pp. 3976–3983, 2015.
- [24] N. Femia, G. Petrone, G. Spagnuolo, and M. Vitelli, "Optimization of perturb and observe maximum power point tracking method," *IEEE Transactions on Power Electronics*, vol. 20, no. 4, pp. 963–973, 2005.
- [25] H. Schmidt, B. Burger, U. Bussemas, and S. Elies, "How fast does an MPP tracker really need to be?," *Proc. 24th EuPVSEC*, pp. 3273–3276, 2009.
- [26] M. Valentini, A. Raducu, D. Sera, and R. Teodorescu, "PV inverter test setup for European efficiency, static and dynamic MPPT efficiency evaluation," 2008 11th International Conference on Optimization of Electrical and Electronic Equipment, pp. 433–438, 2008.



**Faicel El Aamri** received the B.Sc. and M.Sc. degree in electrical engineering from Cadi Ayyad University in 2011 and 2013, he is working currently towards his PhD degree at PhD Center of physics and engineering sciences in Hassan First University.

His area of research interest is control of Grid-connected PV Inverter, power electronic, and Induction Motor Drives.



electronic.

Dr. Hattab is the co-inventor of 1 US patent on "Method and an apparatus for controlling the switches of a Boost converter composed of plural bridge devices".



the Coordinator of the Photovoltaic Systems Research Programme with DET.

His research interests include photovoltaic power systems, specifically in the modeling, characterization, diagnostics, and maximum power point tracking (MPPT) of PV systems, grid integration of PV power and power electronics.



**Sergiu Viorel Spataru** obtained the B.Sc. degree in electrical engineering in 2009, from the "Politehnica" University of Timisoara (UPT), Romania. In 2011 he obtained the M.Sc. degree in wind power systems from Aalborg University, Denmark, where in 2015 he obtained the Ph.D. degree in "Characterization and diagnostic methods for PV modules and arrays".

His current research activities include performance modelling of photovoltaic systems, reliability testing of photovoltaic modules, electroluminescence imaging, modelling and machine learning methods applied to diagnostic and condition monitoring of photovoltaic systems.



**Josep M. Guerrero** (S'01-M'04-SM'08-FM'15) received the B.Sc. degree in telecommunications engineering, the M.Sc. degree in electronics engineering, and the Ph.D. degree in power electronics from the Technical University of Catalonia, Barcelona, in 2000 and 2003, respectively. Since 2011, he has been a Full Professor with the Department of Energy Technology, Aalborg University, Denmark, where he is responsible for the Microgrid Research Program. From 2012, he is a guest Professor at the Chinese Academy of Science and the Nanjing University of Aeronautics and Astronautics, and from 2014, he is a chair Professor in Shandong University.

His research interests are oriented to different microgrid aspects, including power electronics, distributed energy-storage systems, hierarchical and cooperative control, energy management systems, and optimization of microgrids and islanded minigrids. In 2014, he was awarded by Thomson Reuters as ISI Highly Cited Researcher, and in 2015 same year he was elevated to IEEE Fellow for contributions to "distributed power systems and microgrids".



**Azeddine Mouhsen** is Professor of Physics at Hassan First University, Morocco, since 1996. He holds a PhD from Bordeaux University, France in 1995 and a thesis from Moulay Ismail University, Morocco, in 2001. He specializes in Instrumentation and measurements, sensors, applied optics, Energy transfer, radiation-matter Interactions.

Pr. Azeddine has taught courses in physical sensors, chemical sensors, instrumentation, systems technology, digital electronics and industrial data processing. He has published over 20 papers and he is the co-inventor of one patent. Actually he is the Director of Laboratory of radiation - matter & Instrumentation.